Fig. 3. MurJ activity is required for ColM-dependent cleavage of lipid II in spheroplasts. Cells lacking the ColM receptor FhuA and producing the indicated MurJ variants were grown, labeled, and treated with MTSES as for Fig. 1. Spheroplasts were then prepared. In all but one case, spheroplasts were pelleted and resuspended in ColM reaction buffer with sucrose, and MTSES (0.8 mM) was added as indicated. The lysis + sample was resuspended in buffer lacking sucrose to lyse the spheroplasts. ColM (100 µg) was added to the prepared spheroplasts as indicated, and they were incubated for 15 min at 37°C. Lipid intermediates were detected by scintillation counting after butanol extraction. Statistics are as for Fig. 1. cpm, counts per minute.

at positions 29, 49, 263, and 269 rapidly induced lysis, suggesting that MurJ function, and thus PG synthesis, was inhibited (Fig. 2 and fig. S5). In contrast, treatment of MurJ^{E273C} cells with MTSES caused cell shape defects and limited lysis indicative of an incomplete PG synthesis block due to partial MurJ inhibition. The toxicity of MTSES labeling was suppressed in all five strains by the presence of the wild-type *murJ* allele (Fig. 2 and fig. S5). Thus, MTSES specifically and rapidly inhibits these single-Cys MurJ variants. We chose MurJ^{A29C} (Fig. 2, and figs. S6 and S7) to assess the effect of MurJ inactivation on lipid II flipping.

This chemical genetic method for MurJ inactivation was compatible with the in vivo flippase assay. MTSES treatment of MurJ^{WT} cells did not affect lipid II processing by ColM (Fig. 1, B and C, and fig. S1). Additionally, in the absence of MTSES, MurJ^{A29C} cells behaved like MurJ^{WT} cells (Fig. 1, B and C, and fig. S1). However, simultaneous addition of MTSES and ColM to MurJ^{A29C} cells failed to produce significant quantities of the ColM-dependent product PP-M$_{pep4}$-G. In fact, radiolabel in the lipid fraction increased in these samples (Fig. 1, B and C, and fig. S1). Thus, when MurJ^{A29C} was inactivated with MTSES, lipid II was protected from ColM cleavage, and label accumulated in the lipid fraction as observed previously for MurJ-depletion strains (4, 6).

The protection of lipid II from ColM cleavage upon MurJ^{A29C} inactivation suggests that either lipid II is not flipped or that inhibiting MurJ^{A29C}

somehow interferes with ColM import or activity. To investigate this, we performed our assay using spheroplasting to remove the outer membrane (OM) barrier (13) and provide ColM with direct access to flipped lipid II. In the absence of MTSES, ColM treatment of MurJ^{WT} or MurJ^{A29C} spheroplasts reduced the amount of label in the lipid fraction (Fig. 3), indicating that lipid II was actively flipped and thus cleaved by ColM. Although MTSES did not affect ColM activity on MurJ^{WT} spheroplasts, it completely abolished lipid II processing by ColM in MurJ^{A29C} spheroplasts (Fig. 3). Moreover, lysis of MTSES-treated MurJ^{A29C} spheroplasts restored lipid II processing, indicating that the intact IM impeded the access of ColM to lipid II. Thus, MurJ appears to act as a lipid II flippase.

When MurJ^{A29C} was inactivated with MTSES, flippase activity was reduced to a level that was barely detectable and was incompatible with life. This observation indicates that the essential function of MurJ is to translocate lipid II and that other factors catalyzing lipid II flipping are unlikely to exist in *E. coli*. Nevertheless, we investigated the requirement of SEDS proteins for flippase activity by depleting FtsW in a Δ*rodA* strain. We found that lipid II flipping remained robust in this background (figs. S8 and S9). Although it is possible that residual FtsW in these cells was sufficient for the observed activity, this result suggests that SEDS proteins are not responsible for lipid II flippase activity in vivo. Alternatively, the decrease in levels of PG lipid intermediates upon FtsW depletion (fig. S9) suggests that either synthesis of PG precursors or recycling of undecaprenyl-P might be affected by the loss of SEDS activity. From these data and the fact that MurJ contains a central solvent-exposed

cavity that is essential for function (8), we conclude that MurJ is the lipid II flippase in *E. coli*.

REFERENCES AND NOTES

1. A. Typas, M. Banzhaf, C. A. Gross, W. Vollmer, *Nat. Rev. Microbiol.* **10**, 123–136 (2012).
2. A. Bouhss, A. E. Trunkfield, T. D. Bugg, D. Mengin-Lecreulx, *FEMS Microbiol. Rev.* **32**, 208–233 (2008).
3. M. A. de Pedro, W. D. Donachie, J. V. Höltje, H. Schwarz, *J. Bacteriol.* **183**, 4115–4126 (2001).
4. A. Inoue *et al.*, *J. Bacteriol.* **190**, 7298–7301 (2008).
5. M. M. Khattar, K. J. Begg, W. D. Donachie, *J. Bacteriol.* **176**, 7140–7147 (1994).
6. N. Ruiz, *Proc. Natl. Acad. Sci. U.S.A.* **105**, 15553–15557 (2008).
7. R. N. Hvorup *et al.*, *Eur. J. Biochem.* **270**, 799–813 (2003).
8. E. K. Butler, R. M. Davis, V. Bari, P. A. Nicholson, N. Ruiz, *J. Bacteriol.* **195**, 4639–4649 (2013).
9. A. O. Henriques, P. Glaser, P. J. Piggot, C. P. Moran Jr., *Mol. Microbiol.* **28**, 235–247 (1998).
10. T. Mohammadi *et al.*, *EMBO J.* **30**, 1425–1432 (2011).
11. M. El Ghachi *et al.*, *J. Biol. Chem.* **281**, 22761–22772 (2006).
12. T. Touzé *et al.*, *Biochem. Soc. Trans.* **40**, 1522–1527 (2012).
13. L. A. Heppel, *Science* **156**, 1451–1455 (1967).

GENETIC OSCILLATIONS

A Doppler effect in embryonic pattern formation

Daniele Soroldoni,[1,2,3]* **David J. Jörg,**[4]* **Luis G. Morelli,**[1,5] **David L. Richmond,**[1] **Johannes Schindelin,**[1,6] **Frank Jülicher,**[4] **Andrew C. Oates**[1,2,3]†

During embryonic development, temporal and spatial cues are coordinated to generate a segmented body axis. In sequentially segmenting animals, the rhythm of segmentation is reported to be controlled by the time scale of genetic oscillations that periodically trigger new segment formation. However, we present real-time measurements of genetic oscillations in zebrafish embryos showing that their time scale is not sufficient to explain the temporal period of segmentation. A second time scale, the rate of tissue shortening, contributes to the period of segmentation through a Doppler effect. This contribution is modulated by a gradual change in the oscillation profile across the tissue. We conclude that the rhythm of segmentation is an emergent property controlled by the time scale of genetic oscillations, the change of oscillation profile, and tissue shortening.

Segmental patterns are common throughout nature. In animals from diverse phyla, segmentation of the body axis occurs during embryogenesis, and in most cases, segments are added sequentially, with a distinct

period as the body axis elongates. Recent findings indicate that a common mechanism involving genetic oscillations underlies this morphological segmentation in vertebrates and arthropods (1). We investigated how the time scale of

genetic oscillations determines the timing of segmentation.

In sequentially segmenting animals, the unsegmented tissue exhibits patterns of oscillating gene expression reminiscent of waves that travel from the posterior to the anterior, where they arrest. These waves are kinematic and emerge at the tissue level from the coordinated output of cellular genetic oscillators (2–5). This situation is similar to news ticker displays in which a moving pattern is caused by on-and-off switching of individual stationary lamps (6). The sequential

[1]Max Planck Institute of Molecular Cell Biology and Genetics, Pfotenhauerstr 108, 01307 Dresden, Germany. [2]Medical Research Council (MRC)–National Institute for Medical Research, The Ridgeway, Mill Hill, London, NW7 1AA, UK. [3]Department of Cell and Developmental Biology, University College London, Gower Street, London, WC1E 6BT, UK. [4]Max Planck Institute for the Physics of Complex Systems, Nöthnitzer Strasse 38, 01187 Dresden, Germany. [5]Departamento de Física, Facultad de Ciencias Exactas y Naturales, Universidad de Buenos Aires and Instituto de Física de Buenos Aires, Consejo Nacional de Investigaciones Científicas y Técnicas, Pabellón 1, Ciudad Universitaria, 1428 Buenos Aires, Argentina. [6]Laboratory for Optical and Computational Instrumentation, University of Wisconsin at Madison, 271 Animal Sciences, 1675 Observatory Drive, Madison, WI 53706, USA.
*These authors contributed equally to this work. †Corresponding author. E-mail: aoates@nimr.mrc.ac.uk

arrest of the kinematic waves is thought to prefigure the position and set the period of segment formation (7). During vertebrate segmentation, the onset and arrest of these waves are controlled by a complex genetic network that acts in the unsegmented presomitic mesoderm (PSM). The PSM gives rise to the somites, which are the precursors of adult segments (vertebrae, ribs, and associated skeletal muscles). Since its discovery, it has been generally assumed that this network, termed the "segmentation clock," resembles a genetic clock with a single, well-defined period (3). In this simplified picture, both the onset and arrest of the kinematic waves happen with the same period, which is identical to that of segment formation (6–9). However, these fundamental assumptions have not been tested systematically because it has proven difficult to visualize oscillating gene expression in real time and simultaneously quantify the timing of morphological segmentation over a substantial time scale (2, 4, 10).

To this end, we used a transgenesis approach to generate a reliable reporter for the oscillating gene *her1*, named *Looping* (fig. S1), and developed a multidimensional time-lapse setup designed to systematically compare the periods of morphological segmentation and genetic oscilla-

tions in multiple zebrafish embryos (Fig. 1A). Our imaging setup was sensitive enough to detect reporter oscillations in real time and fast enough to simultaneously record segment formation in a population of 20 embryos (Fig. 1B and movie S1). Embryonic growth was not affected by our mounting technique, which ensured that wild-type and transgenic siblings developed normally (fig. S2). With this approach, we observed that multiple kinematic waves (Fig. 1C, color arrowheads, and movie S1) travel from the posterior to anterior PSM at each point in time. As expected, we found that the arrest of reporter oscillations in the anterior PSM coincided with the formation of every new segment (Fig. 1B, arrowhead, and movie S2) (2, 7, 11). As the waves travel along the tissue, their wavelength shortens (Fig. 1C, arrows); thus, the wave pattern can be characterized by the number of waves and by their wavelengths.

To quantify the timing of onset and arrest of kinematic waves, we locally measured the reporter expression in the anterior and the posterior PSM (Fig. 1D, circles). From previous studies, it was unclear whether the posterior PSM oscillates (2, 12). We found that both regions oscillate, although with different reporter amplitudes (Fig. 1D, bottom diagram). We

Fig. 1. Oscillations in the anterior and posterior presomitic mesoderm (PSM) have different periods. (**A**) Mounting of zebrafish embryos for multidimensional imaging. Each time-lapse experiment consists of 20 *xy* positions with a *z* stack (6 slices at 20 μm intervals) to keep the PSM in focus. (**B**) Snapshots from *Looping*, a transgenic reporter of the oscillating gene *her1*, reveal that Her1::YFP (yellow fluorescent protein) fusion protein is confined to the PSM. The white arrowhead marks the most recently formed somite/segment boundary. Scale bar, 100 μm; LUT, high (white) to low (blue) reporter intensity; BF, brightfield. (**C**) Multiple kinematic waves (different colored arrowheads) emerge from the posterior PSM ("P") and travel anteriorly ("A") till they arrest (white arrowhead). (**D**) A region of interest (ROI) interpolator is used to measure the average reporter intensity in the posterior (inset, green circle) and anterior (inset, red circle) PSM. Both regions oscillate but experience a different number of oscillations (annotated with peak number). (**E**) Periods of morphological segmentation ("S") and anterior ("A") oscillations are identical, whereas posterior ("P") oscillations occur significantly slower (~9%). Four independent experiments (*N*), forty individual embryos (*n*), Whiskers min/max (*t* test, Welch correction, ***$P < 0.0001$).
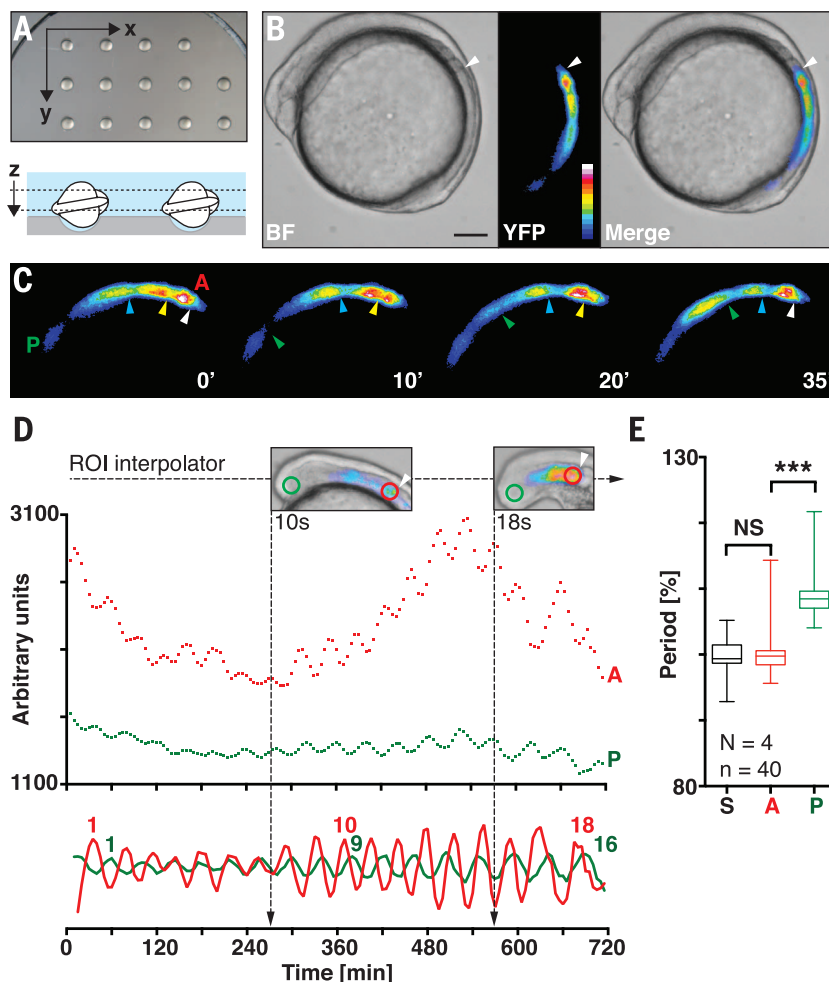
Fig. 2. The wave pattern in the PSM changes continuously as the tissue length decreases. (**A**) A LOI interpolator is used to measure the reporter intensity along the entire PSM and construct a kymograph that captures the trajectories of slowing, kinematic waves (tilted white ridges) and demonstrates the substantial decrease in PSM length. (**B**) Wavelet transformation. Each vertical line of the kymograph (white dotted line) is used to translate amplitude into phase information and construct (**C**) a phase map that is independent of local amplitude fluctuations. (A) and (C) show a single representative embryo. Yellow horizontal lines in a phase map yields the number of kinematic waves at a given time point, which (**D**) decreases with increasing segment number. The local wavelength (distance between purple ticks) also decreases over time. Data are from two independent replicates (*N*), 18 embryos (*n*).
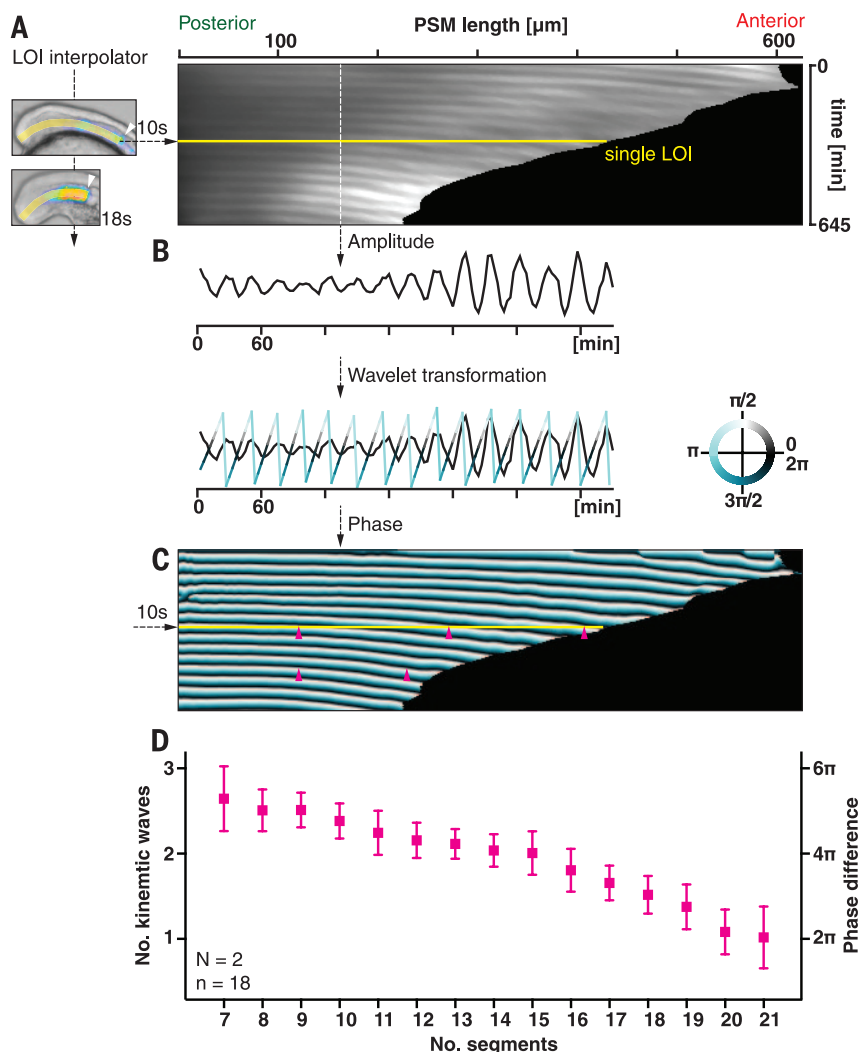
observed that within the same time interval, the number of oscillations in the posterior was smaller than in the anterior: during nine posterior oscillations, 10 oscillations occur in the anterior (Fig. 1D). Consequently, oscillations in the posterior are slower, with an average offset of about 9% (8.8 ± 0.52%, *P* < 0.0001) (Fig. 1E). This finding is not consistent with a single, well-defined period for the segmentation clock. Next, we directly compared the periods of genetic oscillations and segment formation, focusing on the trunk segmentation where the segmentation period is known to be constant (*13*). We found that the period of anterior oscillations is the same as segmentation (Fig. 1E). Thus, the period of segmentation matches the period with which kinematic waves arrest in the anterior but is significantly faster than the period of genetic oscillations in the posterior (Fig. 1E): During nine posterior oscillations, 10 segments are formed.

To understand this paradoxical period offset, we aimed to obtain a comprehensive picture of reporter expression throughout the PSM. To this end, we generated kymographs that display the average reporter intensity along lines

of interest (LOIs) throughout the entire PSM (Fig. 2A). Each horizontal line of pixels in this kymograph represents a LOI at a specific time point, and its length corresponds to the PSM length. Obvious features of all kymographs are the trajectories of kinematic waves and the substantial shortening of the PSM over time (average total shortening is 60% after 13 segments). This implies the relative motion of the anterior end of the PSM, where the waves arrest, toward the posterior end. As a consequence, the anterior end moves into the approaching kinematic waves, shortening the time interval between their onset and arrest. This is reminiscent of the Doppler effect, in which an observer moving toward a sound source perceives an increased sound frequency as compared with what an observer at rest perceives.

In the presence of a Doppler effect, the number of kinematic waves decreases as the tissue shortens (supplementary text). To test this expectation, we analyzed the spatio temporal properties of kinematic waves for a population of embryos by generating phase maps from the intensity kymographs (Fig. 2, B and C; fig. S3; and supplementary text). These phase maps

capture the spatial and temporal dynamics of oscillations while being independent of local amplitude variations (Fig. 2B). A horizontal line of pixels in the phase map captures the profile of phases at a specific time point (Fig. 2C, yellow line); a phase increment of 2π along a horizontal line corresponds to one kinematic wave, and the distance covered by this increment is the local wavelength (Fig. 2C, pink ticks, and movie S3). Therefore, the number of kinematic waves can be determined by the antero-posterior phase difference divided by 2π. These phase maps can be used to determine whether the number of kinematic waves changes over time with a subinteger resolution exceeding that of simple peak counting in a kymograph. We found that the average number of kinematic waves decreases with the number of formed segments (Fig. 2D and movies S4 and S5). Consistent with this analysis, a decrease in the number of kinematic waves can also be observed from snapshots of endogenous oscillating genes in wild-type siblings at successive developmental times (fig. S4). These findings confirm the presence of a Doppler effect.

Such a Doppler effect would not occur if the wave pattern scaled (supplementary text). Scaling

Fig. 3. Doppler and Dynamic Wavelength effects modulate the period of segmentation. (**A**) In the classical Doppler effect, an observer moving toward a sound source perceives an increased sound frequency as compared with what an observer at rest perceives. This is indicated by the larger number of wave peaks (crossing dashed lines) that an observer in motion (red) experiences compared with an observer at rest (green) during the same time interval. (**B**) A dynamic change of the wavelength at the position of an observer at rest (red) can cause a change of the observed period compared with an observer at rest at a different position (green). (**C**) In the zebrafish PSM, in which the anterior end acts as an observer that is moving relative to the kinematic waves, and the wavelength is dynamically changing, these two effects combine and regulate the anterior period (Fig. 2, phase map, in comparison).
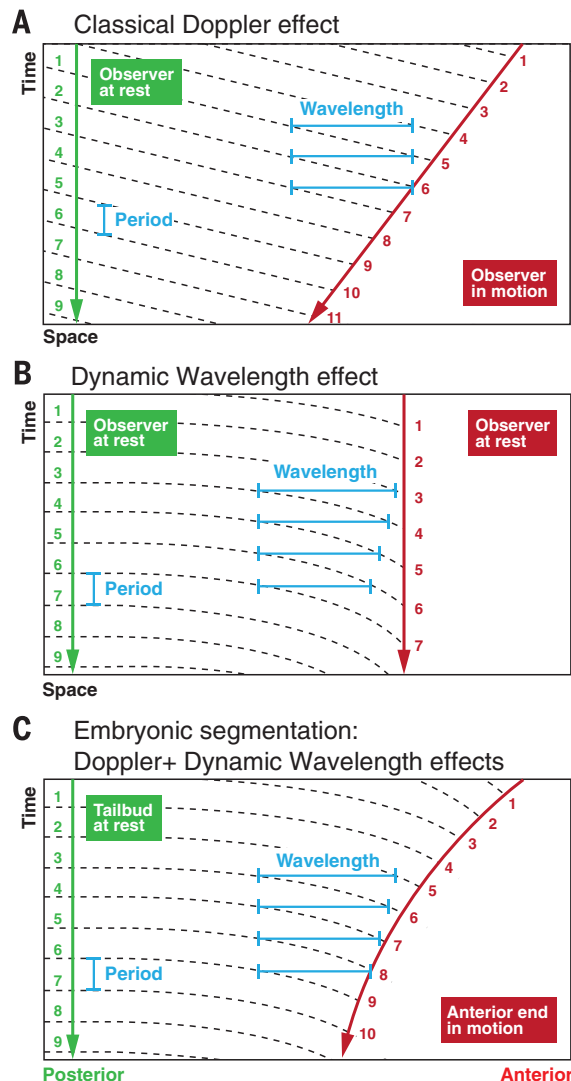
means that the wave pattern shrinks proportionally with the length of the tissue. Such a scaling of the wave pattern has been recently reported in in vitro–cultured mouse PSM explants (*5*) and requires that the number of kinematic waves visible along the PSM remains constant in time. The change in number of waves observed here supports the presence of a Doppler effect and rules out scaling of the wave pattern in zebrafish.

Can we conclude that a Doppler effect alone accounts for the observed decrease in kinematic wave number and the measured period offset? In a classical Doppler effect with only the observer in motion, the wavelength of the sound waves remains constant in time (Fig. 3A). In our analogy, this would imply that the anterior end of the PSM (observer) is in motion while the local wavelength remains constant, resulting in a shortened anterior period. However, from our phase maps we determined that the local wavelength is not constant but decreases over time (Figs. 2C and 3B, figs. S5 and S6, and

supplementary text). This dynamic change of the wavelength tends to prolong the anterior period (Fig. 3B, fig. S7, and supplementary text) and thus opposes the Doppler effect. Hence, the period of segmentation is modulated through the combination of these two opposing effects, the Doppler effect and the dynamic wavelength (Fig. 3C and fig. S7). Although the relative contribution of these effects varies during development, the experimentally observed offset between anterior and posterior period is due to the larger average magnitude of the Doppler compared with the Dynamic Wavelength effect (fig. S7 and supplementary text). The Dynamic Wavelength effect discovered here is a general principle, and there is no reason to assume that it is restricted to the zebrafish PSM. An analogous effect would arise in a wave-carrying medium from a space- and time-dependent change of refraction.

Traditionally, genetic oscillations in the posterior PSM have been viewed as the pacemaker for the segmentation process, which is emphasized

in the term "segmentation clock." Our findings show that the clock metaphor is insufficient to understand the timing of segment formation. In addition to the time scale set by the genetic network controlling the oscillations, the change in length of the PSM and the change of the kinematic wavelength must be included to understand the period of segmentation observed in vivo. The biological mechanisms by which the tissue length and kinematic wavelength change remain open questions. Our work highlights the need to go beyond descriptions of embryonic segmentation that are based on steady-state or scaling conditions and reveals the consequences of the spatial features of the wave pattern for the timing of segmentation.

REFERENCES AND NOTES

1. A. F. Sarrazin, A. D. Peel, M. Averof, *Science* **336**, 338–341 (2012).
2. E. A. Delaune, P. François, N. P. Shih, S. L. Amacher, *Dev. Cell* **23**, 995–1005 (2012).
3. I. Palmeirim, D. Henrique, D. Ish-Horowicz, O. Pourquié, *Cell* **91**, 639–648 (1997).
4. Y. Masamizu *et al.*, *Proc. Natl. Acad. Sci. U.S.A.* **103**, 1313–1318 (2006).
5. V. M. Lauschke, C. D. Tsiairis, P. François, A. Aulehla, *Nature* **493**, 101–105 (2013).
6. A. C. Oates, L. G. Morelli, S. Ares, *Development* **139**, 625–639 (2012).
7. B. Bénazéraf, O. Pourquié, *Annu. Rev. Cell Dev. Biol.* **29**, 1–26 (2013).
8. F. Giudicelli, E. M. Ozbudak, G. J. Wright, J. Lewis, *PLOS Biol.* **5**, e150 (2007).
9. L. G. Morelli *et al.*, *HFSP J* **3**, 55–66 (2009).
10. D. Soroldoni, A. C. Oates, *Curr. Opin. Genet. Dev.* **21**, 600–605 (2011).
11. A. Aulehla *et al.*, *Nat. Cell Biol.* **10**, 186–193 (2008).
12. A. Mara, J. Schroeder, C. Chalouni, S. A. Holley, *Nat. Cell Biol.* **9**, 523–530 (2007).
13. C. Schröter *et al.*, *Dev. Dyn.* **237**, 545–553 (2008).